

Article

Scaling Properties of the Mean Multiplicity and Pseudorapidity Density in $e^- + e^+$, $e^\pm + p$, $p(\bar{p}) + p$, $p + A$ and $A + A(B)$ Collisions

Roy A. Lacey ^{1,2,*} , Peifeng Liu ^{1,2}, Niseem Magdy ¹, Máté Csanád ^{1,3} , Benjamin Schweid ^{1,2}, Nuggehalli N. Ajitanand ¹, John Alexander ¹ and Robert Pak ⁴

¹ Department of Chemistry, Stony Brook University, Stony Brook, NY 11794-3400, USA; peifeng.liu@stonybrook.edu (P.L.); niseem.abdelrahman@stonybrook.edu (N.M.); csanad@elte.hu (M.C.); benjamin.schweid@stonybrook.edu (B.S.); ajit@mail.chem.sunysb.edu (N.N.A.); john.alexander@stonybrook.edu (J.A.)

² Department of Physics, Stony Brook University, Stony Brook, NY 11794-3800, USA

³ Department of Atomic Physics, Eötvös Loránd University, H-1117 Budapest, Pázmány P. s. 1/A, Hungary

⁴ Physics Department, Brookhaven National Laboratory, Upton, New York, NY 11973, USA; pak@bnl.gov

* Correspondence: Roy.Lacey@Stonybrook.edu

Received: 30 November 2017; Accepted: 15 January 2018; Published: 22 January 2018

Abstract: The charged-particle pseudorapidity density ($dN_{\text{ch}}/d\eta$) for $p(\bar{p})+p$, $p+A$ and $A+A(B)$ collisions and the mean multiplicity $\langle N_{\text{ch}} \rangle$ for $e^- + e^+$, $e^\pm + p$, and $p(\bar{p})+p$ collisions are studied for a wide range of beam energies (\sqrt{s}). Characteristic scaling patterns are observed for both $dN_{\text{ch}}/d\eta$ and $\langle N_{\text{ch}} \rangle$, consistent with a thermal particle production mechanism for the bulk of the soft particles created in all of these systems. The scaling patterns found also validate an essential role for quark participants in these collisions. The measured values for $dN_{\text{ch}}/d\eta$ and $\langle N_{\text{ch}} \rangle$ are observed to factorize into contributions that depend on $\log(\sqrt{s})$ and the number of nucleon or quark participant pairs N_{pp} . The quantification of these contributions gives expressions that serve to systematize $dN_{\text{ch}}/d\eta$ and $\langle N_{\text{ch}} \rangle$ measurements spanning nearly 4 orders of magnitude in \sqrt{s} and to predict their values as a function of \sqrt{s} and N_{pp} .

Keywords: multiplicity scaling; leading particle effect; effective energy; participant scaling

1. Introduction

Measurements of particle yields and kinematic distributions in electron–positron ($e^- + e^+$), electron–proton ($e^\pm + p$), proton–proton ($p(\bar{p})+p$), proton–nucleus ($p+A$) and nucleus–nucleus ($A+A(B)$) collisions are essential for characterizing their global properties and to develop a good understanding of the mechanism(s) for particle production [1–9]. The $p+p$ measurements also provide crucial reference data for studies of nuclear-medium effects in $A+A(B)$ and $p+A$ collisions, as well as improved constraints to differentiate between particle production models and to fine-tune event generators.

Particle production in $A+A(B)$ collisions is frequently (but of course not always) described with thermodynamic and hydrodynamical models that utilize macroscopic variables such as the temperature and entropy as model ingredients. This contrasts with the microscopic phenomenology (involving ladders of perturbative gluons, classical random gauge fields or strings, and parton hadronization) often used to characterize the soft collisions that account for the bulk of the particles produced in $e^- + e^+$, $e^\pm + p$, $p(\bar{p})+p$ and $p+A$ collisions [10–14]. The associated mechanisms, commonly classified as single-diffractive (SD) dissociation, double-diffractive (DD) dissociation and

inelastic (INEL) non-diffractive (ND) scattering in $p(\bar{p})+p$ collisions [1], typically do not emphasize the temperature and entropy as model elements.

Despite this predilection to use different theoretical model frameworks for $p(\bar{p})+p$, $p+A$ and $A+A(B)$ collisions, it is well known that similar charged-particle multiplicity (N_{ch}) and pseudorapidity density ($dN_{\text{ch}}/d\eta$) results are obtained in $p(\bar{p})+p$ and peripheral $A+A(B)$ and $p+A$ collisions, as is seen, for example, in measurement results utilized further on in this paper. Moreover, an azimuthal long-range (pseudorapidity difference $|\Delta\eta| \geq 4$) two-particle angular correlation, akin to the “ridge” that results from collective anisotropic flow in $A+A$ collisions, has been observed in $p+p$ and $p+Pb$ collisions at the Large Hadron Collider (LHC) [15–18] and in $d+Au$ and $He+Au$ collisions at Relativistic Heavy Ion Collider (RHIC) [19,20]. Qualitative consistency with these data has also been achieved in initial attempts to describe the amplitudes of these correlations hydrodynamically [19–21]. Thus, an important open question is whether equilibrium dynamics, linked to a common underlying particle production mechanism, dominates for these systems. In this work, we use a large part of the available $dN_{\text{ch}}/d\eta$ measurements for $p+p$, $p+A$ and $A+A(B)$ collisions, as well as the $\langle N_{\text{ch}} \rangle$ measurements for e^-+e^+ , $e^\pm+p$, and $p(\bar{p})+p$ collisions, to search for scaling patterns that could signal such an underlying particle production mechanism.

2. Analysis

Our scaling analysis employs the macroscopic entropy (S) ansatz:

$$S \sim (TR)^3 \sim \text{const.} \quad (1)$$

to capture the underlying physics of particle production, where T is the temperature, and R is a characteristic length related to the volume. This equation is based on the basic thermodynamic relation between the entropy density and temperature. We furthermore assume that $dN_{\text{ch}}/d\eta$ and $\langle N_{\text{ch}} \rangle$ are both proportional to S . A further simplification, $N_{\text{pp}}^{1/3} \propto R$, can be used to relate the number of participant pairs N_{pp} to the initial volume (as is seen in measurements of Bose–Einstein correlations [22]). These pairs can be specified as colliding participant pairs (e.g., $N_{\text{pp}} = 1$ for e^-+e^+ , $e^\pm+p$ and $p(\bar{p})+p$ collisions), nucleon participant pairs ($N_{\text{pp}} = N_{\text{npp}}$) or quark participant pairs ($N_{\text{pp}} = N_{\text{qpp}}$). In heavy-ion physics, N_{npp} is denoted as N_{part} , but this is not to be mixed with our more general notation of N_{pp} . For $p+p$, $p+A$ and $A+A(B)$ collisions, Monte Carlo Glauber calculations [23–28] were performed for several collision centralities at each beam energy to obtain N_{npp} and N_{qpp} . In each of these calculations, a subset $N_{\text{np}} = 2N_{\text{npp}}$ ($N_{\text{qp}} = 2N_{\text{qpp}}$) of the nucleons (quarks) became participants in each collision by undergoing an initial INEL $N+N$ ($q+q$) interaction.

The $N+N$ ($q+q$) cross-sections used in these calculations were obtained from the data systematics reported in [29].

Equation (1) suggests similar characteristic patterns for $[(dN_{\text{ch}}/d\eta)/N_{\text{pp}}]^{1/3}$ and $[\langle N_{\text{ch}} \rangle/N_{\text{pp}}]^{1/3}$ as a function of centrality and collision energy for all the collision systems. We use this scaling ansatz in conjunction with the wealth of measurements spanning several orders of magnitude in \sqrt{s} to search for and study these predicted patterns.

The $\langle N_{\text{ch}} \rangle$ measurements (describing multiplicities extrapolated to the full phase-space) for e^-+e^+ , $e^\pm+p$, and $p(\bar{p})+p$ collisions are shown in Figure 1a. These indicate a nonlinear increase with $\log(\sqrt{s})$, with $\langle N_{\text{ch}} \rangle_{ee} > \langle N_{\text{ch}} \rangle_{pp} > \langle N_{\text{ch}} \rangle_{ep}$ at each value of \sqrt{s} . In contrast, Figure 1b shows a linear increase of $[\langle N_{\text{ch}} \rangle/N_{\text{pp}}]^{1/3}$ ($N_{\text{pp}} = 1$) with $\log(\sqrt{s})$, suggesting a linear increase of T with $\log(\sqrt{s})$. Figure 1b also indicates comparable slopes for $[\langle N_{\text{ch}} \rangle/N_{\text{pp}}]^{1/3}$ versus $\log(\sqrt{s})$ for e^-+e^+ , $e^\pm+p$, and $p(\bar{p})+p$ collisions, albeit with different magnitudes for $[\langle N_{\text{ch}} \rangle/N_{\text{pp}}]^{1/3}$. This similarity is compatible with the notion of an effective energy (E_{eff}) in $p(\bar{p})+p$ and $e^\pm+p$ collisions, available for particle production [30–33]. The remaining energy is associated with the leading particle(s), which emerge at small angles with respect to the beam direction—the “leading particle effect” [34]. In a constituent quark picture [35], only a fraction of the available quarks in $p(\bar{p})+p$ and $e^\pm+p$ collisions

contribute to E_{eff} . Thus, $\kappa_1 \sqrt{s_{ee}} \approx \kappa_2 \sqrt{s_{pp}} \approx \kappa_3 \sqrt{s_{ep}}$ (with $\kappa_1 \equiv 1$) would be expected to give similar values for E_{eff} [36] and hence comparable $\langle N_{\text{ch}} \rangle$ values in $e^- + e^+$, $p(\bar{p}) + p$ and $e^\pm + p$ collisions. Here, $\kappa_{2,3}$ are scale factors that are related to the number of quark participants and hence the fraction of the available c.m energy that contributes to particle production.

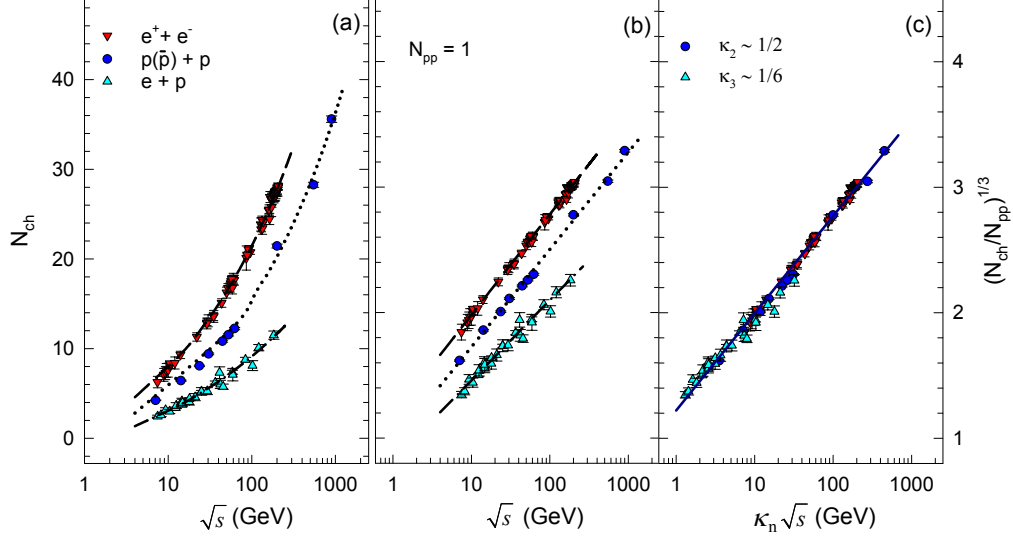


Figure 1. (a) $\langle N_{\text{ch}} \rangle$ vs. collision energy for $e^- + e^+$ [37], $p(\bar{p}) + p$ [38–42] and $e^\pm + p$ [43–45] collisions; (b) $[\langle N_{\text{ch}} \rangle / N_{\text{pp}}]^{1/3}$ vs. collision energy; (c) $[\langle N_{\text{ch}} \rangle / N_{\text{pp}}]^{1/3}$ vs. $\kappa_n \sqrt{s}$ for the κ_n values indicated. The curves are drawn to guide the eye.

Figure 1c validates this leading particle effect through the center of mass collision energy relation stated above. It shows that the disparate magnitudes of $[\langle N_{\text{ch}} \rangle / N_{\text{pp}}]^{1/3}$ versus \sqrt{s} for $e^- + e^+$, $p(\bar{p}) + p$ and $e^\pm + p$ collisions (cf. Figure 1b) scale to a single curve for $[\langle N_{\text{ch}} \rangle / N_{\text{pp}}]^{1/3}$ versus $\kappa_n \sqrt{s}$, where $\kappa_1 = 1$, $\kappa_2 \sim 1/2$ and $\kappa_3 \sim 1/6$. A fit to the data in Figure 1c gives the expression

$$\langle N_{\text{ch}} \rangle = \left[b_{\langle N_{\text{ch}} \rangle} + m_{\langle N_{\text{ch}} \rangle} \log(\kappa_n \sqrt{s}) \right]^3, \quad b_{\langle N_{\text{ch}} \rangle} = 1.22 \pm 0.01, \quad m_{\langle N_{\text{ch}} \rangle} = 0.775 \pm 0.006, \quad (2)$$

which can be used to predict $\langle N_{\text{ch}} \rangle$ as a function of \sqrt{s} for $e^- + e^+$, $e^\pm + p$, and $p(\bar{p}) + p$ collisions.

Figures 2a and 3a show $dN_{\text{ch}}/d\eta|_{\eta \approx 0}$ measurements for INEL and non-single-diffractive (NSD) $p + p$ collisions, respectively, for beam energies spanning the range $\sqrt{s_{\text{NN}}} \sim 15 \text{ GeV} - 13 \text{ TeV}$ (we note that for $p + p$ collisions, $\sqrt{s} = \sqrt{s_{\text{NN}}}$, we however use the latter term to be comparable to $p + A$ and $A + A(B)$ collisions; we note furthermore that for some of the cases, $dN_{\text{ch}}/d\eta|_{|\eta| < 0.5}$; hence here we use the more general $dN_{\text{ch}}/d\eta|_{\eta \approx 0}$ term). These plots indicate a monotonic increase of $dN_{\text{ch}}/d\eta|_{\eta \approx 0}$ with $\sqrt{s_{\text{NN}}}$, similar to that observed for $\langle N_{\text{ch}} \rangle$ in Figure 1a. Figures 2b and 3b, by contrast, confirm the expected linear growth of $[(dN_{\text{ch}}/d\eta|_{\eta \approx 0})/N_{\text{pp}}]^{1/3}$ with $\log(\sqrt{s_{\text{NN}}})$ (where again we make use of the $\sqrt{s} = \sqrt{s_{\text{NN}}}$ relation for $p + p$ collisions). Here the expectation for the linear trend is based on the mean transverse momentum ($\langle p_T \rangle \propto T$) for the particles emitted in these collisions, increasing as $\log(\sqrt{s_{\text{NN}}})$. The open points and dotted curves in these figures affirm the expected trend for the $\sqrt{s_{\text{NN}}}$ dependence of $[(dN_{\text{ch}}/d\eta|_{\eta \approx 0})/N_{\text{pp}}]^{1/3}$. Here, the change in magnitude largely reflects the difference in the proportionality constants for N_{pp} and N_{qpp} (as in $a_{\text{qpp}} N_{\text{qpp}}^{1/3} \propto R$ and $a_{\text{pp}} N_{\text{pp}}^{1/3} \propto R$). The fits, indicated by the dashed curves in Figures 2b and 3b, give the expressions

$$dN_{\text{ch}}/d\eta|_{\text{INEL}} = [b_{\text{INEL}} + m_{\text{INEL}} \log(\sqrt{s_{\text{NN}}})]^3, \quad b_{\text{INEL}} = 0.826 \pm 0.008, \quad m_{\text{INEL}} = 0.220 \pm 0.004 \quad (3)$$

$$dN_{\text{ch}}/d\eta|_{\text{NSD}} = [b_{\text{NSD}} + m_{\text{NSD}} \log(\sqrt{s_{\text{NN}}})]^3, \quad b_{\text{NSD}} = 0.747 \pm 0.022, \quad m_{\text{NSD}} = 0.267 \pm 0.007 \quad (4)$$

for the mid-pseudorapidity density for INEL and NSD p+p collisions. Here, it is noteworthy that the recent INEL p+p measurements at $\sqrt{s_{NN}} = 13$ TeV by the CMS [46] and ALICE [47] collaborations are in very good agreement with the scaling prediction shown in Figure 2b.

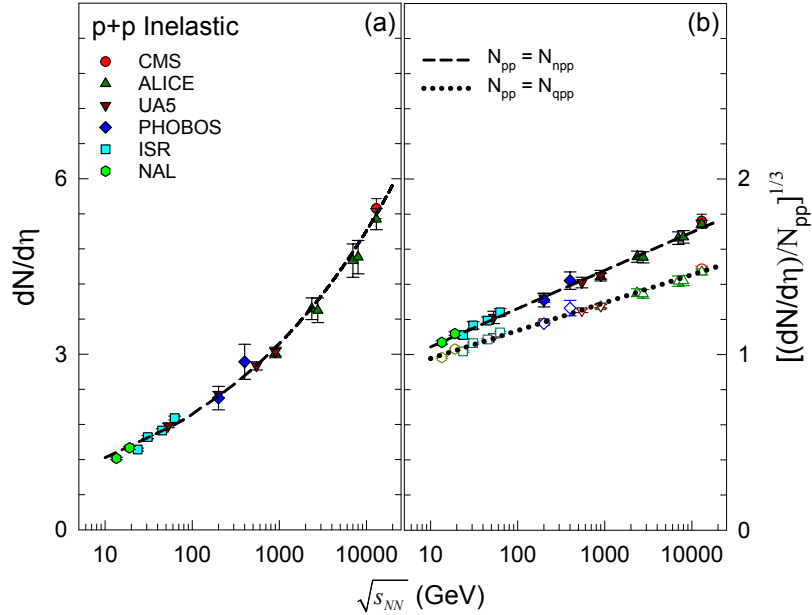


Figure 2. (a) $dN_{ch}/d\eta|_{\eta \approx 0}$ vs. collision energy, and (b) $[(dN_{ch}/d\eta)/N_{pp}]^{1/3}$ vs. collision energy, for p+p inelastic measurements from CMS [46], ALICE [47–49], UA5 [50], PHOBOS [51], ISR [40] and NAL Bubble Chamber [52]. The error bars include systematic uncertainties, when available. The curves in panel (b) represent fits to the data (see text).

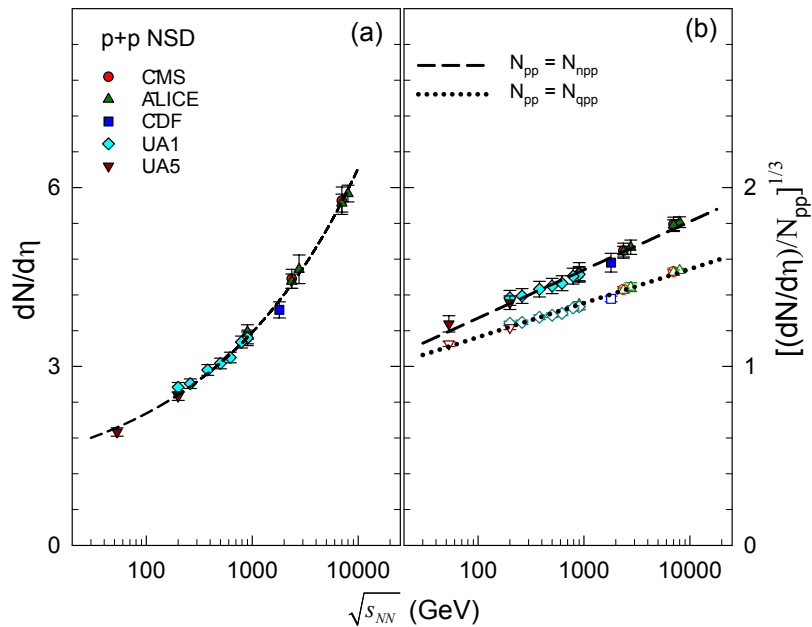


Figure 3. (a) $dN_{ch}/d\eta|_{\eta \approx 0}$ vs. collision energy, and (b) $[(dN_{ch}/d\eta)/N_{npp}]^{1/3}$ vs. collision energy, for p+p non-single-diffractive (NSD) measurements from CMS [53], ALICE [49], CDF [54], UA1 [55] and UA5 [50]. The error bars include the available systematic uncertainties. The curves in panel (b) represent fits to the data (see text).

The scaling properties for p+A and A+A(B) collisions are summarized in Figure 4, where illustrative plots of $[(dN_{\text{ch}}/d\eta|_{|\eta|<0.5})/N_{\text{npp}}]^{1/3}$ versus $dN_{\text{ch}}/d\eta$ and $N_{\text{npp}}^{1/3}$ and $[(dN_{\text{ch}}/d\eta|_{|\eta|<0.5})/N_{\text{qpp}}]^{1/3}$ versus $N_{\text{qpp}}^{1/3}$ are shown. Analogous plots have been obtained for other collision systems and beam energies. We note that in these cases, $|\eta| < 0.5$ was used to determine the pseudorapidity density at midrapidity—unlike the case of the previous figures, where a subscript $\eta \approx 0$ was given. Figure 4a,b shows that, irrespective of the collision system, $[(dN_{\text{ch}}/d\eta|_{|\eta|<0.5})/N_{\text{npp}}]^{1/3}$ increases as $\log(dN_{\text{ch}}/d\eta)$ ($N_{\text{npp}}^{1/3}$), suggesting that T has a logarithmic (linear) dependence on the pseudorapidity density (size) at a given value of $\sqrt{s_{\text{NN}}}$; we note the slope increase with the beam energy, as well as the lack of sensitivity to the system type (Cu+Cu, Cu+Au, Au+Au or U+U), for a fixed value of $\sqrt{s_{\text{NN}}}$. These results suggest that, in addition to the increase with $\sqrt{s_{\text{NN}}}$, the mean transverse momentum $\langle p_T \rangle$ or transverse mass $\langle m_T \rangle$ of the emitted particles should increase as $\log(dN_{\text{ch}}/d\eta)$ at a given value of $\sqrt{s_{\text{NN}}}$ (in line with the ansatz of our paper). These results also suggest that the pseudorapidity density factorizes into contributions that separately depend on $\sqrt{s_{\text{NN}}}$ and $N_{\text{npp}}^{1/3}$.

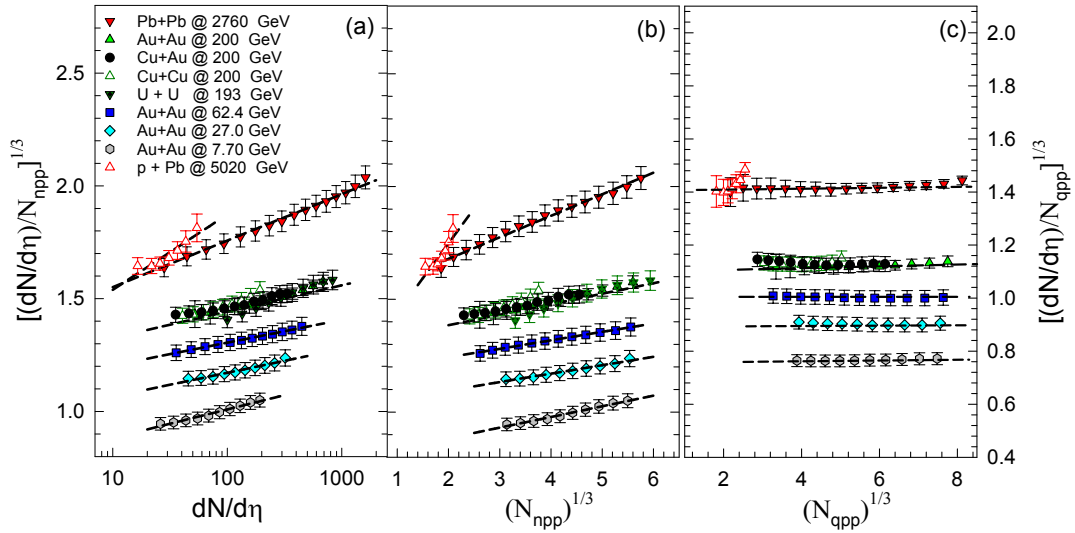


Figure 4. (a) $[(dN_{\text{ch}}/d\eta|_{|\eta|<0.5})/N_{\text{npp}}]^{1/3}$ vs. $dN_{\text{ch}}/d\eta$; (b) $[(dN_{\text{ch}}/d\eta|_{|\eta|<0.5})/N_{\text{npp}}]^{1/3}$ vs. $N_{\text{npp}}^{1/3}$; (c) $[(dN_{\text{ch}}/d\eta|_{|\eta|<0.5})/N_{\text{qpp}}]^{1/3}$ vs. $N_{\text{qpp}}^{1/3}$. Results are shown for several systems and $\sqrt{s_{\text{NN}}}$ values as indicated. The data are obtained from [4–9,56]. The curves are drawn to guide the eye.

Figure 4c contrasts with Figure 4a,b. It shows that, when N_{qpp} is used instead of N_{npp} , the size dependence of $[(dN_{\text{ch}}/d\eta|_{|\eta|<0.5})/N_{\text{npp}}]^{1/3}$ (but not its $\sqrt{s_{\text{NN}}}$ dependence), apparent in Figure 4b, is suppressed. We attribute the flat dependence of $[(dN_{\text{ch}}/d\eta|_{|\eta|<0.5})/N_{\text{qpp}}]^{1/3}$ on the size ($N_{\text{npp}}^{1/3}$ or $N_{\text{qpp}}^{1/3}$) to the linear dependence of $N_{\text{qp}}/N_{\text{npp}}$ on $N_{\text{npp}}^{1/3}$ (related to the initial size), as illustrated in Figure 5a for Pb+Pb and Au+Au collisions. We note that for central and mid-central p+Pb collisions, $N_{\text{qp}}/N_{\text{npp}}$ decreases with $N_{\text{npp}}^{1/3}$; this results in a reduction of the energy released in these collisions, as well as large multiplicity fluctuations.

The $\sqrt{s_{\text{NN}}}$ dependence of $[(dN_{\text{ch}}/d\eta|_{|\eta|<0.5})/N_{\text{qpp}}]^{1/3}$ for A+A(B) and NSD p+p collisions are compared in Figure 5b. The comparison indicates strikingly similar trends for NSD p+p and A+A(B) collisions, as would be expected for a common underlying particle production mechanism in these collisions. We note that for $\sqrt{s_{\text{NN}}} \lesssim 2$ TeV, higher temperatures (and larger $\langle p_T \rangle$) are implied for the smaller p+p collision systems. Figures 4c and 5b also indicate that the centrality and $\sqrt{s_{\text{NN}}}$ -dependent values of $dN_{\text{ch}}/d\eta|_{|\eta|<0.5}$, obtained for different collision systems, scaled as N_{qpp} and $\log(\sqrt{s_{\text{NN}}})$. A fit to the A+A(B) data in Figure 5b gives the expression

$$dN_{\text{ch}}/d\eta|_{|\eta|<0.5} = N_{\text{qpp}} [b_{\text{AA}} + m_{\text{AA}} \ln(\sqrt{s_{\text{NN}}})]^3, \quad b_{\text{AA}} = 0.530 \pm 0.008, \quad m_{\text{AA}} = 0.113 \pm 0.002 \quad (5)$$

which systematizes the collision energy and centrality dependencies of the pseudorapidity density in A+A(B) collisions across the full range of beam energies. Equation (5) provides a basis for robust predictions of the value of $dN_{ch}/d\eta|_{|\eta|<0.5}$ as a function of N_{pp} and \sqrt{s} across systems and collision energies. For example, it predicts a $\sim 20\%$ increase in the $dN_{ch}/d\eta|_{|\eta|<0.5}$ values for Pb+Pb collisions (across centralities) at 5.02 TeV, compared to the same measurement at 2.76 TeV. This increase reflects the respective contributions linked to the increase in the value of $\sqrt{s_{NN}}$ and the small growth in the magnitudes of N_{pp} .

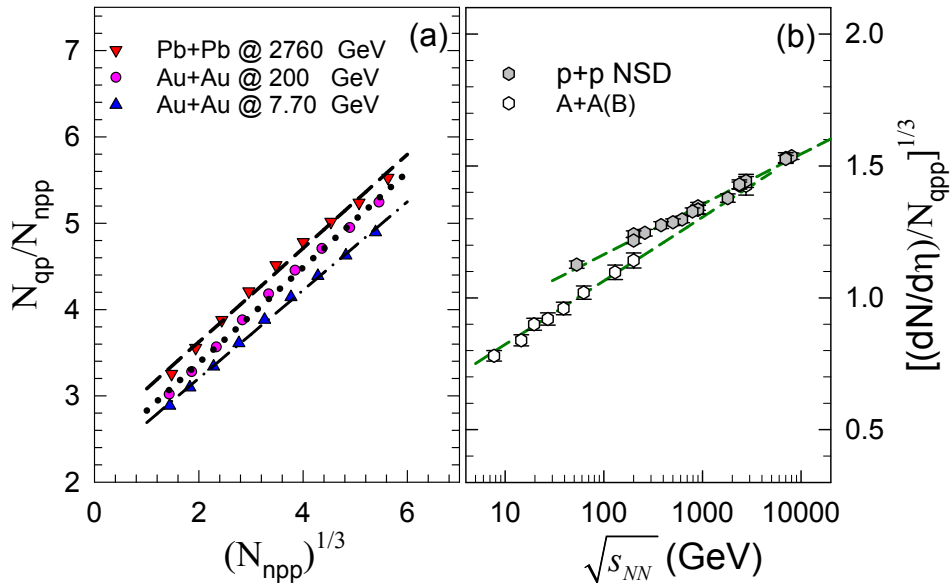


Figure 5. (a) N_{qp}/N_{npp} vs. $N_{npp}^{1/3}$ for Au+Au and Pb+Pb collisions; (b) $[(dN_{ch}/d\eta|_{|\eta|<0.5})/N_{pp}]^{1/3}$ vs. $\sqrt{s_{NN}}$ for non-single-diffractive (NSD) p+p and A+A(B) collisions as indicated.

3. Summary

In summary, we have performed a systematic study of the scaling properties of $dN_{ch}/d\eta$ measurements for p+p, p+A and A+A(B) collisions and $\langle N_{ch} \rangle$ measurements for e^-+e^+ , $e^\pm+p$, and $p(\bar{p})+p$ collisions, to investigate the mechanisms for particle production in these collisions. The wealth of the measurements, spanning several orders of magnitude in collision energy, indicates characteristic scaling patterns for both $dN_{ch}/d\eta$ and $\langle N_{ch} \rangle$, suggestive of a common underlying entropy production mechanism for these systems. The scaling patterns for $\langle N_{ch} \rangle$ validate the essential role of the leading particle effect in $p(\bar{p})+p$ and $e^\pm+p$ collisions and the importance of quark participants in A+A(B) collisions. The patterns for the scaled values of $dN_{ch}/d\eta$ and $\langle N_{ch} \rangle$ indicate fairly similar trends for NSD p+p and A+A(B) collisions and show that the pseudorapidity density and $\langle N_{ch} \rangle$ for e^-+e^+ , $e^\pm+p$, p+p, and A+A(B) collisions factorize into contributions that depend on $\log(\sqrt{s})$ and N_{pp} , respectively. The quantification of these scaling patterns gives expressions that serve to systematize the $dN_{ch}/d\eta$ and $\langle N_{ch} \rangle$ measurements for e^-+e^+ , $e^\pm+p$, $p(\bar{p})+p$, p+A and A+A(B) collisions and to predict their magnitudes as a function of N_{pp} and \sqrt{s} . These scaling results have an important utility in the study of a broad array of observables that are currently being pursued at both RHIC and the LHC.

Acknowledgments: This research is supported by the US DOE under contract DE-FG02-87ER40331.A008, as well as the Hungarian NKIFH Grant Nos. FK-123842 and FK-123959. M. Csanád was supported by the ÚNKP-17-4 New National Excellence Program of the Hungarian Ministry of Human Capacities.

Author Contributions: R.A.L. conceived the analysis and wrote most of the paper. M.C. adapted the paper for proceedings publication. In other respects, authors contributed equally to the paper.

Conflicts of Interest: The authors declare no conflict of interest.

References

1. Kittel, W.; De Wolf, E.A. *Soft Multihadron Dynamics*; World Scientific: Hackensack, NJ, USA, 2005.
2. Armesto, N.; Borghini, N.; Jeon, S.; Wiedemann, U.A.; Abreu, S.; Akkelin, V.; Alam, J.; Albacete, J.L.; Andronic, A.; Antonov, D.; et al. Heavy Ion Collisions at the LHC—Last Call for Predictions. *J. Phys.* **2008**, *35*, 054001.
3. Grosse-Oetringhaus, J.F.; Reygers, K. Charged-Particle Multiplicity in Proton-Proton Collisions. *J. Phys.* **2010**, *37*, 083001.
4. Alver, B.; Back, B.B.; Baker, M.D.; Ballintijn, M.; Barton, D.S.; Betts, R.R.; Bickley, A.A.; Bindel, R.; Budzanowski, A.; Busza, W.; et al. Phobos results on charged particle multiplicity and pseudorapidity distributions in Au+Au, Cu+Cu, d+Au, and p+p collisions at ultra-relativistic energies. *Phys. Rev.* **2011**, *83*, 024913.
5. Aamodt, K. Centrality dependence of the charged-particle multiplicity density at mid-rapidity in Pb-Pb collisions at $\sqrt{s_{NN}} = 2.76$ TeV. *Phys. Rev. Lett.* **2011**, *106*, 032301.
6. Chatrchyan, S. Dependence on pseudorapidity and centrality of charged hadron production in PbPb collisions at a nucleon-nucleon centre-of-mass energy of 2.76 TeV. *J. High Energy Phys.* **2011**, *08*, 141.
7. Aad, G. Measurement of the centrality dependence of the charged particle pseudorapidity distribution in lead-lead collisions at $\sqrt{s_{NN}} = 2.76$ TeV with the ATLAS detector. *Phys. Lett.* **2012**, *B710*, 363–382.
8. Adamczyk, L. Inclusive charged hadron elliptic flow in Au + Au collisions at $\sqrt{s_{NN}} = 7.7\text{--}39$ GeV. *Phys. Rev.* **2012**, *86*, 054908.
9. Adare, A.; Afanasiev, S.; Aidala, C.; Ajitanand, N.N.; Akiba, Y.; Akimoto, R.; Al-Bataineh, H.; Alexander, J.; Alfred, M.; Al-Jamel, A.; et al. Transverse energy production and charged-particle multiplicity at midrapidity in various systems from $\sqrt{s_{NN}} = 7.7$ to 200 GeV. *Phys. Rev.* **2016**, *93*, 024901.
10. Kharzeev, D.; Levin, E.; Nardi, M. Color glass condensate at the LHC: Hadron multiplicities in pp, pA and AA collisions. *Nucl. Phys.* **2005**, *747*, 609–629.
11. Armesto, N.; Salgado, C.A.; Wiedemann, U.A. Relating high-energy lepton-hadron, proton-nucleus and nucleus-nucleus collisions through geometric scaling. *Phys. Rev. Lett.* **2005**, *94*, 022002.
12. Albrow, M.G.; Begel, M.; Bourilkov, D.; Campanelli, M.; Chlebana, F.; De Roeck, A.; Dittmann, J.R.; Ellis, S.D.; Field, B.; Field, R.; et al. Tevatron-for-LHC Report of the QCD Working Group. *arXiv* **2006**, arXiv:hep-ph/0610012.
13. Werner, K. The hadronic interaction model EPOS. *Nucl. Phys. Proc. Suppl.* **2008**, *175–176*, 81–87.
14. Dusling, K.; Venugopalan, R. Explanation of systematics of CMS p+Pb high multiplicity di-hadron data at $\sqrt{s_{NN}} = 5.02$ TeV. *Phys. Rev.* **2013**, *D87*, 054014.
15. Khachatryan, V. Observation of Long-Range Near-Side Angular Correlations in Proton-Proton Collisions at the LHC. *J. High Energy Phys.* **2010**, *1009*, 091.
16. Abelev, B.; Adam, J.; Admove, D.; Anare, A.M.; Aggarwal, M.; Rinella, G.A.; Agnello, M.; Agocs, A.G.; Agostinelli, A.; Ahammed, Z.; et al. Long-range angular correlations on the near and away side in p-Pb collisions at $\sqrt{s_{NN}} = 5.02$ TeV. *Phys. Lett.* **2013**, *B719*, 29–41.
17. Aad, G.; Abajyan, T.; Abbott, B.; Abdallah, J.; Abdel Khalek, S.; Abdelalim, A.A.; Abidinov, O.; Aben, R.; Abi, B.; Abolins, M.; et al. Observation of Associated Near-Side and Away-Side Long-Range Correlations in $\sqrt{s_{NN}} = 5.02$ TeV Proton-Lead Collisions with the ATLAS Detector. *Phys. Rev. Lett.* **2013**, *110*, 182302.
18. Chatrchyan, S.; Khachatryan, V.; Sirunyan, A.M.; Tumasyan, A. Observation of long-range near-side angular correlations in proton-lead collisions at the LHC. *Phys. Lett.* **2013**, *B718*, 795–814.
19. Adare, A.; Aidala, C.; Ajitanand, N.N.; Zhou, S. Measurement of long-range angular correlation and quadrupole anisotropy of pions and (anti)protons in central d+Au collisions at $\sqrt{s_{NN}}=200$ GeV. *Phys. Rev. Lett.* **2015**, *114*, 192301.
20. Adare, A.; Afanasiev, S.; Aidala, C.; Ajitanand, N.N.; Akiba, Y.; Akimoto, R.; Al-Bataineh, H.; Alexander, J.; Alfred, M.; Al-Ta'ani, H.; et al. Measurements of elliptic and triangular flow in high-multiplicity $^3\text{He}+\text{Au}$ collisions at $\sqrt{s_{NN}} = 200$ GeV. *Phys. Rev. Lett.* **2015**, *115*, 142301.
21. Bozek, P. Collective flow in p-Pb and d-Pd collisions at TeV energies. *Phys. Rev.* **2012**, *C85*, 014911.
22. Adler, S.S.; Afanasiev, S.; Aidala, C.; Ajitanand, N.N.; Akiba, Y.; Alexander, J.; Amirkas, R.; Aphetche, L.; Aronson, S.H.; Averbek, R.; et al. Bose-Einstein correlations of charged pion pairs in Au + Au collisions at $\sqrt{s_{NN}} = 200$ GeV. *Phys. Rev. Lett.* **2004**, *93*, 152302.

23. Miller, M.L.; Reygers, K.; Sanders, S.J.; Steinberg, P. Glauber modeling in high energy nuclear collisions. *Ann. Rev. Nucl. Part. Sci.* **2007**, *57*, 205–243.
24. Lacey, R.A.; Wei, R.; Ajitanand, N.N.; Taranenko, A. Initial eccentricity fluctuations and their relation to higher-order flow harmonics. *Phys. Rev.* **2011**, *C83*, 044902.
25. Eremin, S.; Voloshin, S. Nucleon participants or quark participants? *Phys. Rev.* **2003**, *C67*, 064905.
26. Bialas, A.; Bzdak, A. Wounded quarks and diquarks in heavy ion collisions. *Phys. Lett.* **2007**, *B649*, 263–268.
27. Nouicer, R. Charged particle multiplicities in A+A and p^+p collisions in the constituent quarks framework. *Eur. Phys. J.* **2007**, *C49*, 281–286.
28. Adler, S.S. Transverse-energy distributions at midrapidity in p+p, d+Au, and Au+Au collisions at $\sqrt{s_{NN}} = 62.4$ –200 GeV and implications for particle-production models. *Phys. Rev.* **2014**, *C89*, 044905.
29. Fagundes, D.A.; Menon, M.J.; Silva, P.V.R.G. On the rise of the proton-proton cross-sections at high energies. *J. Phys.* **2013**, *G40*, 065005.
30. Feinberg, E.L. Multiple production of hadrons at cosmic ray energies (experimental results and theoretical concepts). *Phys. Rept.* **1972**, *5*, 237–350.
31. Albini, E.; Capiluppi, P.; Giacomelli, G.; Rossi, A.M. Mean Charged Hadron Multiplicities in High-Energy Collisions. *Nuovo Cim.* **1976**, *A32*, 101.
32. Basile, M. Evidence of the Same Multiparticle Production Mechanism in p p Collisions as in e^+e^- Annihilation. *Phys. Lett.* **1980**, *92B*, 367.
33. Basile, M. A Detailed Study of Average Charged Particle Multiplicity Versus Available Energy and Invariant Mass at Different \sqrt{s} in pp Interactions. *Nuovo Cim.* **1982**, *A67*, 244.
34. Back, B.B. Comparison of the total charged particle multiplicity in high-energy heavy ion collisions with e^+e^- and p p/anti-p p data. *arXiv* **2003**, arXiv:nucl-ex/0301017.
35. Nyiri, J. Quark structure of hadrons and high-energy collisions. *Int. J. Mod. Phys.* **2003**, *A18*, 2403–2458.
36. Sarkisyan, E.K.G.; Sakharov, A.S. On similarities of bulk observables in nuclear and particle collisions. *arXiv* **2004**, arXiv:hep-ph/0410324.
37. Nakamura, K.; Particle Data Group. Review of particle physics. *J. Phys.* **2010**, *G37*, 075021.
38. Benecke, J.; Blobel, V.; Breitenlohner, P.; Fesefeldt, H.; Heilmann, H.G.; Idschok, U. Rapidity Gap Separation and Study of Single Diffraction Dissociation in p p Collisions at 12-GeV/c and 24-GeV/c. *Nucl. Phys.* **1974**, *B76*, 29–47.
39. Morse, W.M.; Barnes, V.E.; Carmony, D.D.; Christian, R.S.; Garfinkel, A.F.; Rangan, L.K.; Erwin, A.R.; Harvey, E.H.; Loveless, R.J.; Thompson, M.A. π^+p , K^+p and p p Topological Cross-Sections and Inclusive Interactions at 100-GeV Using a Hybrid Bubble Chamber-Spark Chamber System and a Tagged Beam. *Phys. Rev.* **1977**, *D15*, 66.
40. Breakstone, A. Charged Multiplicity Distribution in p p Interactions at ISR Energies. *Phys. Rev.* **1984**, *D30*, 528.
41. Alner, G.J. Scaling Violations in Multiplicity Distributions at 200-GeV and 900-GeV. *Phys. Lett.* **1986**, *167B*, 476–480.
42. Anson, R.E. Charged Particle Multiplicity Distributions at 200-GeV and 900-GeV Center-Of-Mass Energy. *Z. Phys.* **1989**, *C43*, 357.
43. Adloff, C. Evolution of e p fragmentation and multiplicity distributions in the Breit frame. *Nucl. Phys.* **1997**, *B504*, 3–23.
44. Breitweg, J. Measurement of multiplicity and momentum spectra in the current and target regions of the Breit frame in deep inelastic scattering at HERA. *Eur. Phys. J.* **1999**, *C11*, 251–270.
45. Chekanov, S. Multiplicity moments in deep inelastic scattering at HERA. *Phys. Lett.* **2001**, *B510*, 36–54.
46. Khachatryan, V. Pseudorapidity distribution of charged hadrons in proton-proton collisions at $\sqrt{s} = 13$ TeV. *Phys. Lett.* **2015**, *B751*, 143–163.
47. Adam, J. Pseudorapidity and transverse-momentum distributions of charged particles in proton-proton collisions at $\sqrt{s} = 13$ TeV. *Phys. Lett.* **2016**, *B753*, 319–329.
48. Aamodt, K. Charged-particle multiplicity measurement in proton-proton collisions at $\sqrt{s} = 0.9$ and 2.36 TeV with ALICE at LHC. *Eur. Phys. J.* **2010**, *C68*, 89–108.
49. Adam, J. Charged-particle multiplicities in proton-proton collisions at $\sqrt{s} = 0.9$ to 8 TeV. *Eur. Phys. J.* **2017**, *C77*, 33.
50. Alner, G.J. Scaling of Pseudorapidity Distributions at c.m. Energies Up to 0.9-TeV. *Z. Phys.* **1986**, *C33*, 1–6.

51. Nouicer, R. Pseudorapidity distributions of charged particles in d + Au and p + p collisions at $\sqrt{s_{NN}} = 200$ -GeV. *J. Phys.* **2004**, *G30*, S1133–S1138.
52. Whitmore, J. Experimental Results on Strong Interactions in the NAL Hydrogen Bubble Chamber. *Phys. Rept.* **1974**, *10*, 273–373.
53. Khachatryan, V. Transverse-momentum and pseudorapidity distributions of charged hadrons in *pp* collisions at $\sqrt{s} = 7$ TeV. *Phys. Rev. Lett.* **2010**, *105*, 022002.
54. Abe, F. Pseudorapidity distributions of charged particles produced in $\bar{p}p$ interactions at $\sqrt{s} = 630$ GeV and 1800 GeV. *Phys. Rev.* **1990**, *D41*, 2330.
55. Albajar, C. A Study of the General Characteristics of $p\bar{p}$ Collisions at $\sqrt{s} = 0.2$ -TeV to 0.9-TeV. *Nucl. Phys.* **1990**, *B335*, 261–287.
56. Aad, G. Measurement of the centrality dependence of the charged-particle pseudorapidity distribution in proton-lead collisions at $\sqrt{s_{NN}} = 5.02$ TeV with the ATLAS detector. *Eur. Phys. J.* **2016**, *76*, 199.



© 2018 by the authors. Licensee MDPI, Basel, Switzerland. This article is an open access article distributed under the terms and conditions of the Creative Commons Attribution (CC BY) license (<http://creativecommons.org/licenses/by/4.0/>).